Earthq Eng & Eng Vib (2009) 8: 359-371 **DOI**: 10.1007/s11803-009-9004-9

Mathematical modeling and full-scale shaking table tests for multi-curve buckling restrained braces

C. S. Tsai[1†], Yungchang Lin[2‡], Wenshin Chen[2‡] and H. C. Su[3§]

1. *Department of Civil Engineering, Feng Chia University, Taichung, Chinese Taipei*
2. *Graduate Institute of Civil and Hydraulic Engineering, Feng Chia University, Taichung, Chinese Taipei*
3. *Department of Water Resources Engineering and Conservation, Feng Chia University, Taichung, Chinese Taipei*

Abstract: Buckling restrained braces (BRBs) have been widely applied in seismic mitigation since they were introduced in the 1970s. However, traditional BRBs have several disadvantages caused by using a steel tube to envelope the mortar to prevent the core plate from buckling, such as: complex interfaces between the materials used, uncertain precision, and time consumption during the manufacturing processes. In this study, a new device called the multi-curve buckling restrained brace (MC-BRB) is proposed to overcome these disadvantages. The new device consists of a core plate with multiple neck portions assembled to form multiple energy dissipation segments, and the enlarged segment, lateral support elements and constraining elements to prevent the BRB from buckling. The enlarged segment located in the middle of the core plate can be welded to the lateral support and constraining elements to increase buckling resistance and to prevent them from sliding during earthquakes. Component tests and a series of shaking table tests on a full-scale steel structure equipped with MC-BRBs were carried out to investigate the behavior and capability of this new BRB design for seismic mitigation. The experimental results illustrate that the MC-BRB possesses a stable mechanical behavior under cyclic loadings and provides good protection to structures during earthquakes. Also, a mathematical model has been developed to simulate the mechanical characteristics of BRBs.

Keywords: buckling restrained brace; energy absorption; passive control; earthquake energy; plasticity model; structural control; multi-curve BRB

1 Introduction

Traditionally, concentrically braced and eccentrically braced systems are usually used to enhance the earthquake resistance of structures. However, the force redistribution due to the buckling of brace systems results in earthquake energy concentration on certain floors that leads to destruction during earthquakes. To prevent the brace from buckling, considerable research has been conducted since the 1970s that studied different materials and BRB designs. Wakabayashi *et al*. (1973) conducted a component test of the buckling restrained brace (BRB), using different de-bonding materials between the brace and the restrained material to reduce the friction. Kimura *et al*. (1976) tested a steel brace encased in a mortar-filled steel tube subjected to cyclic loadings. Wada *et al*. (1992) reported that the BRB can be designed as a damper to dissipate energy induced by earthquakes. Merritt *et al.* (2003) carried out standard and low-cycle fatigue tests for BRBs to examine their behavior according to the SEAOC-AISC (2002) Recommended Provisions for Buckling-Restrained Braced Frames.

In general, previous research generated outstanding experimental results with regard to the component tests performed for the development of BRBs (Black *et al*., 2002, 2004; Merritt *et al*., 2003; Tsai *et al.*, 2004, 2006; Ma *et al.* 2008). However, very few attempts have been made to investigate the seismic performance of structures equipped with BRBs via shaking table tests, and other issues still need to be addressed, as stated by Tsai *et al*. (2005 and 2008). The de-bonding material between the core plate and the restrained material in the traditional BRB is used to reduce the shear transfer from the core plate to the filled mortar and the steel tube, and also to prevent large differences between the tensile and compressive forces. However, it is difficult to assure that the de-bonding material is still on the core plate surface during the manufacturing process (passing the core plate through the steel tube and pouring the mortar). In addition, the mortar used to resist lateral buckling requires a specific curing time to become strong, and the quality of mortar poured is not easy to determine beforehand without testing. Furthermore, traditional

Correspondence to: C. S. Tsai, Department of Civil Engineering, Feng Chia University, Taichung, Chinese Taipei
Tel: 886-4-24517250 ext.3121
E-mail: cstsai@fcu.edu.tw
†Professor; ‡PhD Candidate; §Assistant Professor

Supported by: Science Council in Chinese Taipei Under Grant No. NSC 94-2211-E-035-015
Received January 6, 2009; **Accepted** March 23, 2009

BRB manufacturing procedures are complex and time consuming due to the manufacturing interfaces for different materials that include steel, mortar, de-bonding material and glue material. In this case, quality and precision are difficult to control. The material used to glue the de-bonding material on the surface of the core plate might be damaged by the high temperatures caused by fire or welding. It might lose the ability to hold the steel tube and mortar, causing them to slide down. In earthquake situations, the de-bonding material may lose its function during the elongation and contraction of the core plate, thereby causing the steel tube and the filled mortar to slide.

To overcome the disadvantages of traditional BRBs,. a new device named the multi-curve buckling restrained brace (MC-BRB) is proposed in this study. The MC-BRB, using only steel materials, includes a core plate, lateral support element, and a constraining element that may be any shape in cross section, such as a rectangular box, double channel, I section, etc. The core plate absorbs the energy induced by earthquakes and may consist of several energy dissipation segments as shown in Figs.1 to 5. As shown in Figs.1 and 2, two energy dissipation segments are combined to form one enlarged segment. These segments are shorter than the traditional BRB, with a single segment for the same length of the core plate. The enlarged segment in the middle of the core plate can be welded to the constraining elements and the lateral support elements because of the symmetry of the axial force and deformation at the middle point in the longitudinal direction. Therefore, by reducing the effective buckling length of the core plate, the buckling strength of the MC-BRB is higher than the traditional BRB and the strain of the MC-BRB in the core plate is larger than the traditional BRB for an identical displacement. Also, no relative displacement occurs between the core plate and the constraining element to cause sliding of constraining and lateral support elements during earthquakes. Therefore, the MC-BRB provides more opportunities to absorb seismic energy and is more stable mechanically than traditional BRBs.

Furthermore, the steel lateral support element and constraining element are used to resist the lateral buckling of the core plate. As shown in Fig. 3, the only clearance that is needed to accommodate the lateral expansion due to the effect of Poisson's ratio when in compression is between the core plate and the lateral support element. No clearance is needed between the

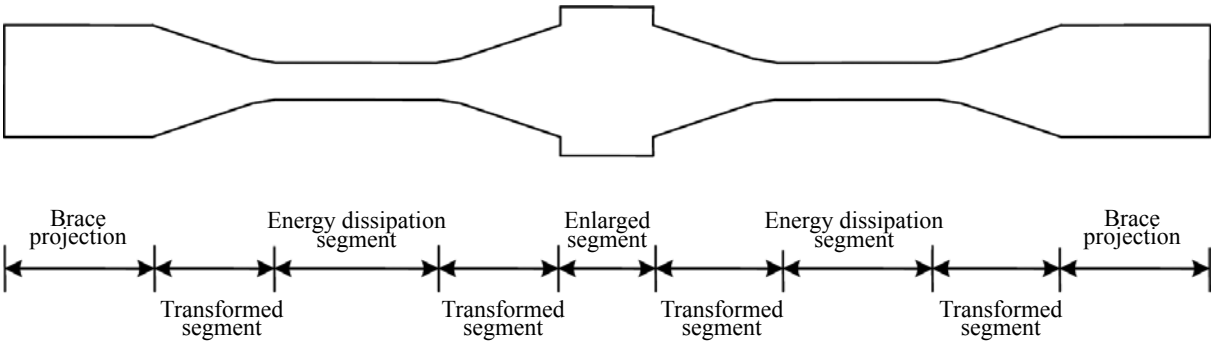

Fig. 1 Flat core plate of MC-BRB

core plate and the constraining element because the thickness of the core plate is much smaller than the core plate width, and the lateral expansion in the thickness direction of the core plate is accommodated by the deformation of the walls of the constraining elements. Also, no de-bonding material is required between the core plate, lateral support elements and constraining elements. The manufacturing procedures, as shown in Fig. 3 for the MC-BRB with a flat core plate, are very simple and include: (1) cutting the core plate and the lateral support element, which may be cut from a single plate; (2) arranging the constraining element, core plate, and lateral support element; and (3) using simple welding technology to connect the lateral support elements, constraining elements, and the enlarged segment (only the middle part) of the core plate.

Fig. 4 shows cross sections of other configurations of the MC-BRB, with double flat core plates or a cruciform

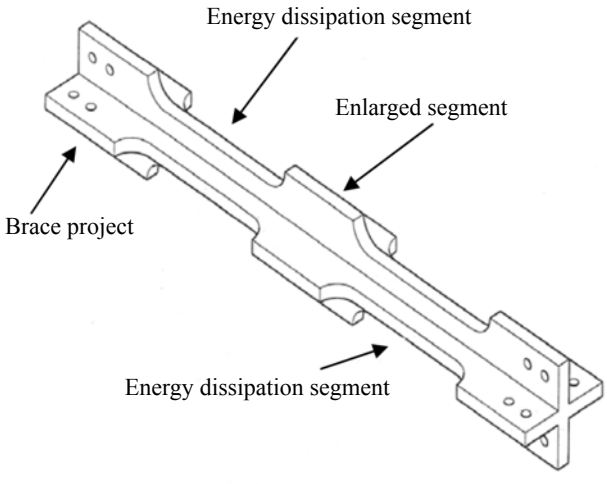

Fig. 2 Cruciform core plate of MC-BRB

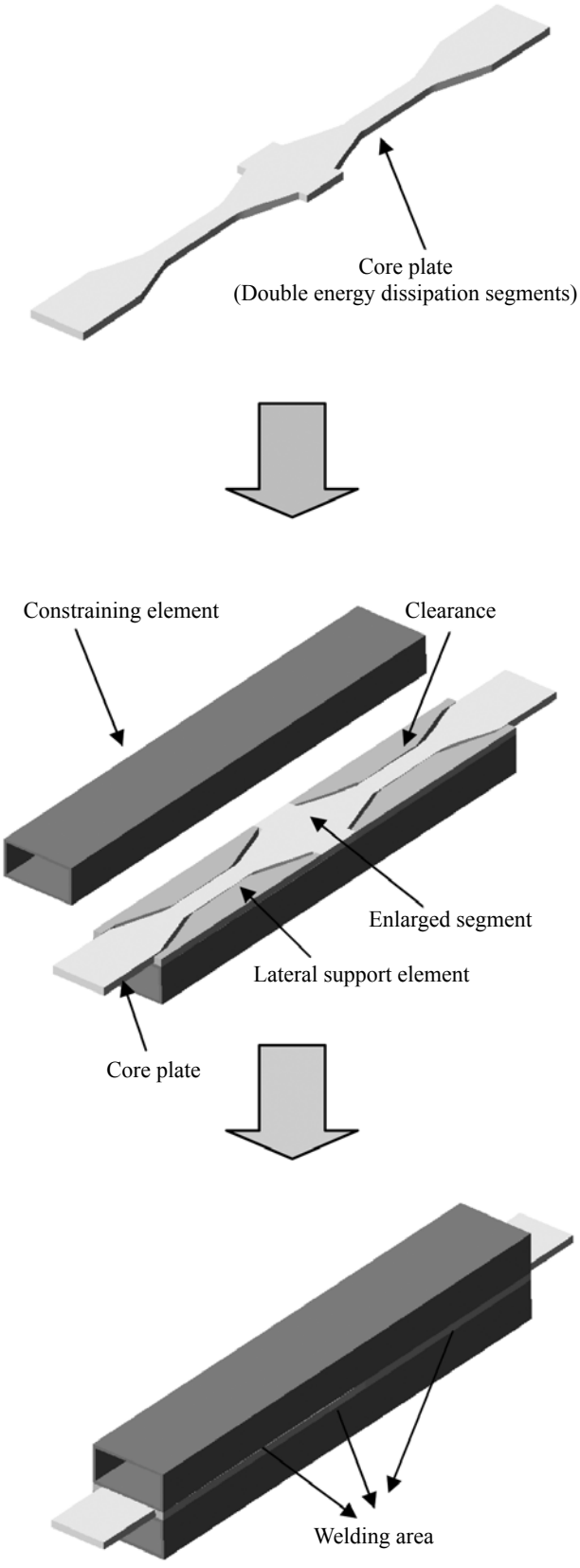

Fig. 3 Manufacturing procedures of MC-BRB

core plate. The first row in Fig. 4 presents three types of cross sections of three MC-BRB configurations, with double flat core plates for the MC-BRB. Figure 5 displays some other types of flat core plates for the MC-BRB. Note that the proposed multi-curve core plates shown in Figs. 1-5 are suitable not only for the use of traditional BRBs with the filled mortar and de-bonding material, but also for all-steel BRBs. The proposed MC-BRB can also be designed by either lengthening the enlarged segment or increasing the number of enlarged segments to achieve a similar effect for the case where several shorter, traditional BRBs are connected in series to reduce the effective buckling length of the core plate.

To examine the behavior and seismic mitigation capability of the MC-BRB under cyclic loadings, component tests and a series of shaking table tests on a full-scale three-story structure equipped with MC-BRBs were carried out at the NCREE. Results of the component tests illustrate that the MC-BRB possesses a stable behavior under cyclic loadings. The shaking table test results demonstrate that the MC-BRB installed in the structure provides good protection from earthquake damage. Furthermore, based on plasticity theory, a two-surface model (Tsai and Chen, 2004) was adopted to simulate the mechanical characteristics of the MC-BRB under cyclic loading, and the response of structures equipped MC-BRBs. Numerical results are in good agreement with experimental results from the component tests and shaking table tests for the full-scale steel structure equipped with MC-BRBs.

2 Mechanical behavior of MC-BRB

As shown in Fig. 6, the axial deformation of the multi-curve reinforced BRB can be determined by integrating all segments of the entire length of the steel core. The deformations for different segments can be derived as follows (Tsai *et al*., 2006).

The deformation in segment 1-1 is given by

$$\Delta_1 = \int_{L_2+L_3}^{L_1+L_2+L_3} \varepsilon_1 \mathrm{d}x = \frac{PL_1}{EA_1} \tag{1}$$

The deformation in segment 2-2 is obtained as

$$\Delta_2 = \int_{L_3}^{L_2+L_3} \varepsilon_2 \mathrm{d}x = \frac{PL_2}{E(A_1 - A_3)} (\ln A_1 - \ln A_3) \tag{2}$$

The deformation in segment 3-3 is given by

$$\Delta_3 = \int_0^{L_3} \varepsilon_3 \mathrm{d}x = \int_0^{L_3} \frac{P}{EA_3} \mathrm{d}x = \frac{PL_3}{EA_3} \tag{3}$$

The deformation in segment 4-4 is given by

$$\Delta_4 = \int_{L_3+L_2+L_1+L_5}^{L_3+L_2+L_1+L_5+L_4} \varepsilon_4 \mathrm{d}x = \frac{PL_4}{EA_4} \tag{4}$$

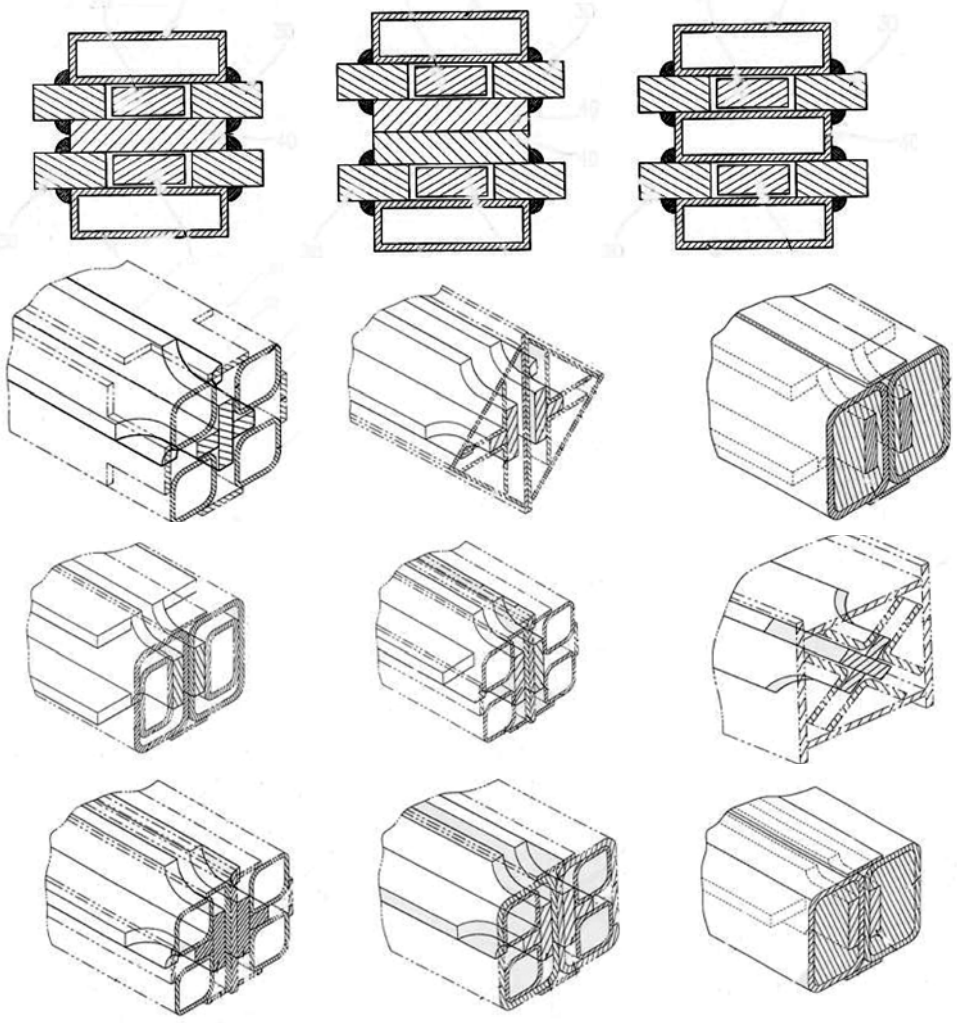

Fig. 4 Types of cross section of MC-BRB (Double flat core plates in the first row)

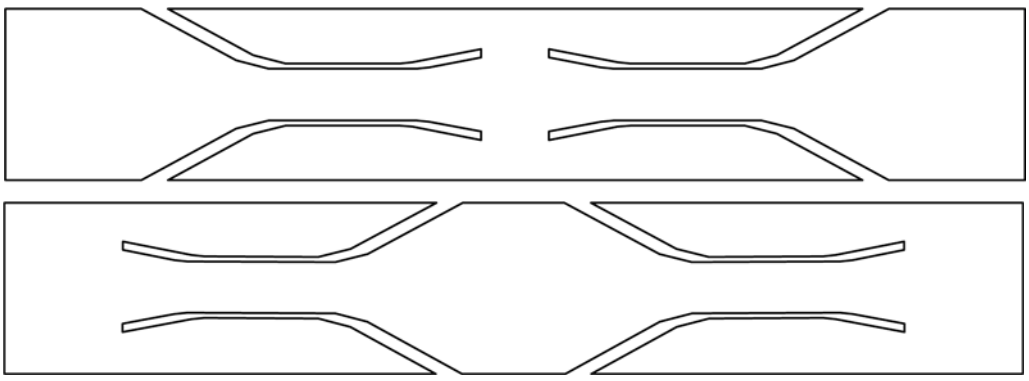

Fig. 5 Types of flat core plate for MC-BRB

The deformation in segment 5-5 is expressed as

$$\Delta_5 = \int_{L_3+L_2+L_1}^{L_3+L_2+L_1+L_5} \varepsilon_5 \mathrm{d}x = \frac{PL_5}{E(A_m - A_1)}(\ln A_\mathrm{m} - \ln A_1) \qquad (5)$$

where L_1, L_2, L_3, L_4 and L_5 are the lengths of segments 1-1, 2-2, 3-3, 4-4 and 5-5, respectively; A_1, A_3 and A_4 are the cross-sectional areas of segments 1-1, 3-3 and 4-4, respectively; and A_m is the largest cross-sectional area of segment 5-5. P is the axial force of the member, and E is the modulus of elasticity.

Due to the connection series for segments in the steel core, the stiffness of the entire MC-BRB can be obtained as:

$$k_{\mathrm{e}}^{\mathrm{a}} = \frac{k_1 k_2 k_3 k_4 k_5}{\left(2k_2 k_3 k_4 k_5 + 2k_1 k_3 k_4 k_5 + 2k_1 k_2 k_4 k_5 + 2k_1 k_2 k_3 k_4 + k_1 k_2 k_3 k_5\right)} \tag{6}$$

where

$$k_1 = \frac{EA_1}{L_1}, k_3 = \frac{EA_3}{L_3}, k_4 = \frac{EA_4}{L_4}; \quad k_2 = \frac{E(A_1 - A_3)}{L_2(\ln A_1 - \ln A_3)};$$

and $k_5 = \dfrac{E(A_{\mathrm{m}} - A_1)}{L_5(\ln A_{\mathrm{m}} - \ln A_1)}$

In traditional BRBs, only one energy dissipation segment is selected without an enlarged segment. Therefore, the traditional BRB is a special case of the proposed MC-BRB by setting the stiffness of the enlarged segment K_4 equal to the energy dissipation segment K_1 and the stiffness of segment 5-5, K_5, equal to K_1. The buckling resistance and stiffness of the MC-BRB are higher than those of the traditional BRB as a result of the enlarged segment.

3 Two-surface model for the MC-BRB

In order to predict the nonlinear behavior of the MC-BRB, a two-surface model based on plasticity theory is introduced to simulate the behavior of the MC-BRB under cyclic loadings (Tsai and Chen, 2004; Tsai *et al*., 2004). As shown in Fig. 7, the yield and bounding surfaces are assumed to follow the kinematic and isotropic hardening rules, respectively. The material behavior will be purely elastic when the stress resultant (force) falls within the yield surface. Changes in the generalized plastic modulus will be obtained by a related shape factor, while the stress resultant is located on the yield surface and moves toward the bounding surface.

Since the MC-BRB is subjected only to axial stress, the stress resultant $\boldsymbol{F}$ at the cross section of the core plate can be written as

$$\boldsymbol{F} = [P] \tag{7}$$

where P is the axial force in the MC-BRB.

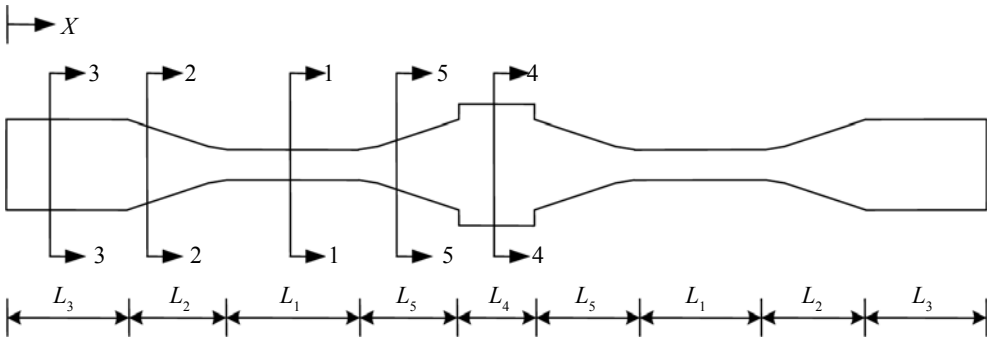

Fig. 6 Sketch of the steel core of the MC-BRB

If ϕ is the yield function in the force space for the core plate, the outward normal direction to the yield surface is given by

$$\boldsymbol{n} = \frac{\phi_{,F}}{\left[\phi_{,F}^{\mathrm{T}} \quad \phi_{,F}\right]^{1/2}} \tag{8}$$

where

$$\phi_{,F} = \frac{\partial \phi}{\partial P} \tag{9}$$

and $\boldsymbol{n}$ = unit outward vector normal to the yield surface.

In accordance with the normality rule, the plastic deformation increment $\mathrm{d}\boldsymbol{u}_{\mathrm{p}}$ is defined as

$$\mathrm{d}\boldsymbol{u}_{\mathrm{p}} = \boldsymbol{n}\mathrm{d}u_{\mathrm{p}} \tag{10}$$

where $\mathrm{d}u_{\mathrm{p}}$ is the magnitude of the plastic deformation.

The normal component of the stress resultant

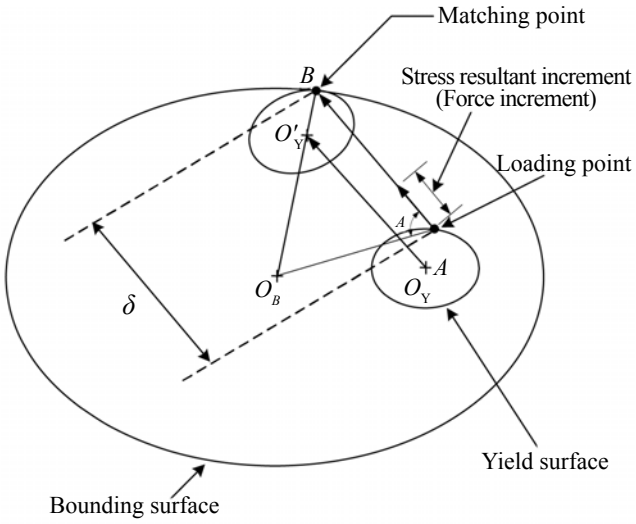

Fig. 7 Two-surface model for nonlinear plasticity

increment, defined as $\mathrm{d}\boldsymbol{F}_{\mathrm{n}}$ can be expressed as

$$\mathrm{d}\boldsymbol{F}_{\mathrm{n}} = \boldsymbol{n}(\boldsymbol{n}^{\mathrm{T}}\mathrm{d}\boldsymbol{F}) \tag{11}$$

By assuming that the relationship between the stress resultant increment in the normal direction $\mathrm{d}\boldsymbol{F}_{\mathrm{n}}$ and the plastic deformation $\mathrm{d}\boldsymbol{u}_{\mathrm{p}}$ follows the flow rule, it can be written as

$$\mathrm{d}\boldsymbol{F}_{\mathrm{n}} = \boldsymbol{K}_{\mathrm{p}}\mathrm{d}\boldsymbol{u}_{\mathrm{p}} \tag{12}$$

and

$$\boldsymbol{K}_{\mathrm{p}} = K_{\mathrm{p}}^{\mathrm{a}} \tag{13}$$

where $K_{\mathrm{p}}^{\mathrm{a}}$ is the plastic modulus in the axial direction, which can be determined from an experimentally established force-deformation relationship.

Since the projection of the tangential component of the stress resultant increment in the normal direction vanishes, the following equation can be defined

$$\boldsymbol{n}^{\mathrm{T}}\mathrm{d}\boldsymbol{F}_{\mathrm{n}} = \boldsymbol{n}^{\mathrm{T}}\mathrm{d}\boldsymbol{F} \tag{14}$$

Substituting Eqs. (10) and (14) into Eq. (12) and rearranging the result yields

$$\mathrm{d}u_{\mathrm{p}} = \frac{\boldsymbol{n}^{\mathrm{T}}\mathrm{d}\boldsymbol{F}}{\boldsymbol{n}^{\mathrm{T}}\boldsymbol{K}_{\mathrm{p}}\boldsymbol{n}} \tag{15}$$

Substitution of Eq. (15) into Eq. (10) leads to

$$\mathrm{d}\boldsymbol{u}_{\mathrm{p}} = \frac{\boldsymbol{n}\boldsymbol{n}^{\mathrm{T}}}{\boldsymbol{n}^{\mathrm{T}}\boldsymbol{K}_{\mathrm{p}}\boldsymbol{n}}\mathrm{d}\boldsymbol{F} \tag{16}$$

According to the deformation decomposition principle, the total deformation $\mathrm{d}\boldsymbol{u}$ of the MC-BRB can be decomposed into an elastic part $\mathrm{d}\boldsymbol{u}_{\mathrm{e}}$ and a plastic part $\mathrm{d}\boldsymbol{u}_{\mathrm{p}}$. Therefore, the total deformation can be written as

$$\mathrm{d}\boldsymbol{u} = \mathrm{d}\boldsymbol{u}_{\mathrm{e}} + \mathrm{d}\boldsymbol{u}_{\mathrm{p}} \tag{17}$$

Moreover, the elastic part must follow Hooke's law; therefore, the relationship between the increments of the elastic deformation and the force can be expressed as

$$\mathrm{d}\boldsymbol{F} = \boldsymbol{K}_{\mathrm{e}}\mathrm{d}\boldsymbol{u}_{\mathrm{e}} \tag{18}$$

and

$$\boldsymbol{K}_{\mathrm{e}} = K_{\mathrm{e}}^{\mathrm{a}} \tag{19}$$

where K_{e}^{a} indicates the elastic rigidity of the MC-BRB in the axial direction.

Substituting Eqs. (16) and (17) into Eq. (18) results in

$$\mathrm{d}\boldsymbol{F} = \boldsymbol{K}_{\mathrm{e}}\mathrm{d}\boldsymbol{u}_{\mathrm{e}} = \boldsymbol{K}_{\mathrm{e}}(\mathrm{d}\boldsymbol{u} - \mathrm{d}\boldsymbol{u}_{\mathrm{p}}) = \boldsymbol{K}_{\mathrm{e}}\mathrm{d}\boldsymbol{u} - \boldsymbol{K}_{\mathrm{e}}\frac{\boldsymbol{n}\boldsymbol{n}^{\mathrm{T}}}{\boldsymbol{n}^{\mathrm{T}}\boldsymbol{K}_{\mathrm{p}}\boldsymbol{n}}\mathrm{d}\boldsymbol{F} \tag{20}$$

Pre-multiplication of Eq. (20) by $\boldsymbol{n}^{\mathrm{T}}$ yields

$$\boldsymbol{n}^{\mathrm{T}}\mathrm{d}\boldsymbol{F} = \frac{\boldsymbol{n}^{\mathrm{T}}\boldsymbol{K}_{\mathrm{e}}\mathrm{d}\boldsymbol{u}}{(1+\dfrac{\boldsymbol{n}^{\mathrm{T}}\boldsymbol{K}_{\mathrm{e}}\boldsymbol{n}}{\boldsymbol{n}^{\mathrm{T}}\boldsymbol{K}_{\mathrm{p}}\boldsymbol{n}})} \tag{21}$$

Substituting Eq. (21) in Eq. (20) leads to

$$\mathrm{d}\boldsymbol{F} = \boldsymbol{K}_{\mathrm{e}}\mathrm{d}\boldsymbol{u}_{\mathrm{e}} = \boldsymbol{K}_{\mathrm{e}}\mathrm{d}\boldsymbol{u} - \frac{\boldsymbol{K}_{\mathrm{e}}\boldsymbol{n}\boldsymbol{n}^{\mathrm{T}}\boldsymbol{K}_{\mathrm{e}}}{(\boldsymbol{n}^{\mathrm{T}}\boldsymbol{K}_{\mathrm{e}}\boldsymbol{n} + \boldsymbol{n}^{\mathrm{T}}\boldsymbol{K}_{\mathrm{p}}\boldsymbol{n})}\mathrm{d}\boldsymbol{u} = \boldsymbol{K}_{\mathrm{ep}}\mathrm{d}\boldsymbol{u} \tag{22}$$

where $\boldsymbol{K}_{\mathrm{ep}}$ is the modified stiffness of $\boldsymbol{K}_{\mathrm{e}}$ for the MC-BRB due to the plastic flow and can be expressed as

$$\boldsymbol{K}_{\mathrm{ep}} = \boldsymbol{K}_{\mathrm{e}} - \frac{\boldsymbol{K}_{\mathrm{e}}\boldsymbol{n}\boldsymbol{n}^{\mathrm{T}}\boldsymbol{K}_{\mathrm{e}}}{(\boldsymbol{n}^{\mathrm{T}}\boldsymbol{K}_{\mathrm{e}}\boldsymbol{n} + \boldsymbol{n}^{\mathrm{T}}\boldsymbol{K}_{\mathrm{p}}\boldsymbol{n})} \tag{23}$$

It is assumed that the yield function of the MC-BRB, ϕ, is given by

$$\phi = a(\frac{P}{P_{\mathrm{p}}} - \frac{X_1}{P_{\mathrm{p}}})^2 - \kappa_\beta^2 = 0 \tag{24}$$

where $\phi_{,F}$ can be expressed as

$$\phi_{,F} = \frac{2a}{P_{\mathrm{p}}}(\frac{P}{P_{\mathrm{p}}} - \frac{X_1}{P_{\mathrm{p}}}) \tag{25}$$

and P_{p} indicates the axial yield force of the MC-BRB, X_1 is the location of the center of the yield surface in the axial direction, and κ_β is the radius of the yield surface.

If $N = [\phi_{,F}^{\mathrm{T}} \quad \phi_{,F}]^{1/2}$ is defined, then the unit normal direction $\boldsymbol{n}$ can be expressed as

$$\boldsymbol{n} = \frac{1}{N}\frac{2a}{P_{\mathrm{p}}}(\frac{P}{P_{\mathrm{p}}} - \frac{X_1}{P_{\mathrm{p}}}) \tag{26}$$

Let $S = \boldsymbol{n}^{\mathrm{T}}\boldsymbol{K}_{\mathrm{e}}\boldsymbol{n} + \boldsymbol{n}^{\mathrm{T}}\boldsymbol{K}_{\mathrm{p}}\boldsymbol{n}$, then

$$S = n^2(K_{\mathrm{e}}^{\mathrm{a}} + K_{\mathrm{p}}^{\mathrm{a}}) \tag{27}$$

Substituting Eqs. (19), (13), and Eqs. (25), (27) into Eq. (23), the modified stiffness of the MC-BRB can be expressed as

$$K_{\mathrm{ep}} = K_{\mathrm{e}}^{\mathrm{a}} - \frac{(nK_{\mathrm{e}}^{\mathrm{a}})^2}{S} \tag{28}$$

As shown in Fig. 7, the distance δ between the loading and matching points on the yield and bounding surfaces, respectively, is given by

$$\delta = \frac{-(F_i\dot{F}_i) + \sqrt{(F_i\dot{F}_i)^2 - (\dot{F}_i\dot{F}_i)(F_iF_i - F_B^2)}}{\sqrt{\dot{F}_i\dot{F}_i}}, \quad i = 1 \tag{29}$$

where $F_1 = P/P_p$, $\dot{F}_1 = dP/P_p$, and F_B is the current size of the bounding surface.

When the stress resultant is on the yield surface and approaching the bounding surface, the plastic modulus of the MC-BRB can be expressed as

$$K_p^P = (1 + h_1' \frac{\delta}{\delta_{ini} - \delta})(K_0)_p^P; \quad h_1' = \frac{A_1}{\delta_{ini}^2} \tag{30}$$

where δ_{ini} is the initial distance between the loading and matching points as the MC-BRB starts yielding; $(K_0)_p^P$, the plastic modulus of the MC-BRB related to the bounding surface, and A_1, the unknown coefficient related to the sharp factor to be determined from the experimental results by applying the curve fitting method. h_1' can also be determined from the experiment.

Furthermore, it was concluded from extensive research (Phillips and Lee, 1979; Tseng and Lee, 1983; Tsai and Chen, 2004; Tsai *et al*., 2004) that the moving direction of the yield surface is parallel to the moving direction of the stress resultant. As shown in Fig. 7, the center of the yield surface moves from O_Y to O_Y', when the stress resultant moves from the loading point on the yield surface to the matching point on the bounding surface. If l_i indicates a component of the unit vector of the stress resultant increment, this component of the unit vector v_i in the direction from O_Y to O_Y' can be obtained as

$$v_i = \frac{1}{L}\left[\frac{(F_B - F_Y)(F_i + \delta l_i)}{\left[(F_j + \delta l_j)(F_j + \delta l_j)\right]^{1/2}} - \alpha_i\right], \quad i = 1 \tag{31}$$

where L is the distance between the points O_Y and O_Y', F_y is the size of the yield surface, and α_i indicates the coordinate of the center of the yield surface in the force space. If $d\alpha_i$ is defined as a moving increment of the center of the yield surface, then according to the consistency rule and Eq. (31) will yield the following equation:

$$|d\alpha| = \frac{A^*(dP/P_p)}{A^* v_1} \tag{32}$$

and

$$d\alpha_1 = |d\alpha| v_1 \tag{33}$$

where

$$A^* = 2a\left(\frac{P}{P_p} - \frac{X_1}{P_p}\right) \tag{34}$$

and dP is the axial force increment in the MC-BRB.

4 Component tests of MC-BRB

To investigate the mechanical behavior of the MC-BRB, component tests were carried out in the Department of Civil Engineering, Feng Chia University, Taichung, Chinese Taipei. The load cell installed on the MTS machine has a maximum capacity of 25 tons. To measure the actual deformation of the MC-BRB, the LVDT was also installed laterally on the specimens. The dimensions of the MC-BRB are listed in Table 1. The yield forces of the specimens were 4 tons and 6 tons and the width of the energy dissipation segments were 20 mm and 30 mm, respectively. In addition, the length of each energy dissipation segment of the MC-BRB was 100 mm.

According to the draft Recommend Provisions for Buckling Restrained Braces (SEAOC-AISC, 2001), designed braces should be tested in accordance with the procedures, and acceptance criteria, and accepted displacements shown in Table 2. Following the testing and applying the calculation method in the provision, the accumulative inelastic deformation was determined to be 272 Δ_{by}, greater than the value of 140 Δ_{by} required in the code. Δ_{by} is defined as the axial deformation of the BRB specimen at the first significant yield.

Figure 8 shows a comparison between the analytical and experimental results. Note that the proposed MC-BRB possesses stable behavior under cyclic loadings at a maximum strain above 2%, and that the proposed mathematical model derived in Section 3 can well simulate the mechanical behavior of the MC-BRB device.

Table 1 Dimensions of the core plates of MC-BRBs mm

Yield force	Each brace projection			Each transformed segment		
	Length	Width	Thickness	Length	Width	Thickness
4 tons	80	60	8	60	60–20	8
6 tons	80	60	8	60	60–30	8
Yield force	Each energy dissipated segment			Enlarged segment		
	Length	Width	Thickness	Length	Width	Thickness
4 tons	100	20	8	50	80	8
6 tons	100	30	8	50	80	8

Note: here 1 ton = 9.81 ×10^3 N

Table 2 Testing procedures of multi-curve buckling restrained brace

Step	Cycles	Deformation	(Accumulative inelastic deformation) / (Δ_{by})
1	6	Δ_{by}	0
2	4	0.5 Δ_{bm}	16
3	4	1.0 Δ_{bm}	64
4	4	1.5 Δ_{bm}	144
5	2	2.0 Δ_{bm}	200
6	2	2.5 Δ_{bm}	272

Note: $\Delta_{bm} = 4\,\Delta_{by}$; Δ_{by} = 0.5 mm

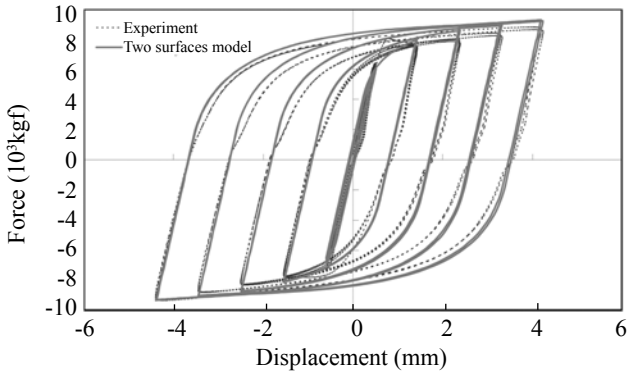

Fig. 8 Comparison between experiment and simulation of multi-curve BRB with yield force of 6 tons

The cross-sectional area of the core plate was increased due to lateral expansion as a result of the Poisson's ratio effect when the BRB was subjected to a compressive load, and the cross-sectional area was reduced due to lateral contraction when in tension. Therefore, the tensile force was less than the compressive force under an identical displacement. Table 3 shows a comparison between the maximum tensile and compressive forces of the MC-BRB under cyclic loadings during component tests, and the comparative results indicate that the distinction between these two forces was smaller than 9%. After satisfying the test procedures recommended by SEAOC-AISC, the specimens were continuously tested until failure. A fracture occurred in the middle part of the energy dissipation segment, as shown in Fig. 9.

Table 3 Comparison between tensile and compressive forces

Specimen	Compression (kgf)	Tension (kgf)	Distinction(%)
MC-BRB_4 tons	6444.37	5938.68	8.5
MC-BRB_6 tons	9342.66	8800.71	6.2

Note: 1 kgf = 9.81 N

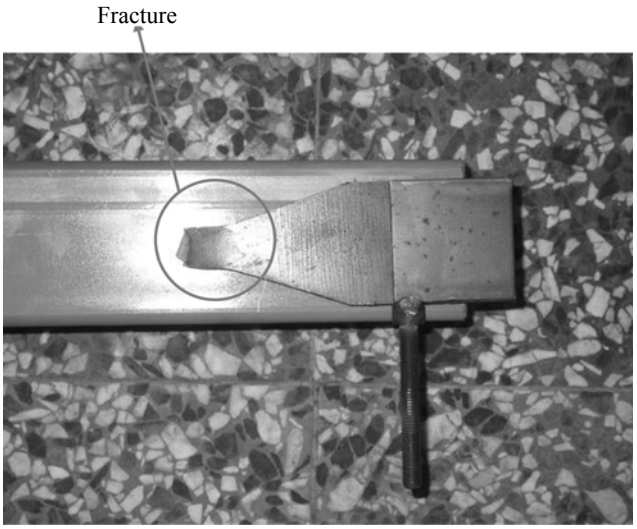

Fig. 9 Fracture in the middle of energy dissipation segment

5 Shaking table tests and numerical analyses of a full-scale three-story steel structure with MC-BRBs

To examine the effectiveness of the MC-BRB in seismic mitigation, a series of shaking table tests of a full-scale structure equipped with MC-BRBs were carried out at the NCREE, Taiwan. As shown in Fig. 10, the tested structure was a full-scale three-story steel structure, with dimensions of 4.5 m and 3.0 m in the longitudinal (*X*-) and lateral (*Y*-) directions, respectively; the height of each story was 3.0 m; and the cross-sections of the beams and columns were H200 × 150 × 6 × 9 mm and H200 × 204 × 12 × 12 mm, respectively. In addition, additional weight of approximately 6936 kg was added to each floor to simulate the load on the floor. In this study, the tri-directional El Centro and Chi-Chi earthquakes (TCU084 station) were utilized and four

Fig. 10 Full-scale steel structure equipped with MC-BRBs

MC-BRBs were positioned on each floor, as shown in Fig.10. Figures 11 and 12 sketch the dimensions of the MC-BRBs used in the *X*- and *Y*-directions of the tested structure, respectively. The installation of the MC-BRBs to the full-scale steel structure for the experiments is shown in Figs. 13 (a) and (b).

In theory, the average yield force of the MC-BRBs installed in the *X*-direction of the tested structure was 17.7 tons and 14.65 tons in the *Y*-direction. The yield deformation of the MC-BRB in the *X*-direction was 4.11 mm and 6.296 mm in the *Y*-direction. During seismic tests, the measured average maximum inter-story shear force for each MC-BRB was 14.2 and 11.99 tons in the *X*- and *Y*-directions, respectively, and inter-story displacement was 5.46 mm in the *X*-direction and 8.2 mm in the *Y*-direction. These inter-story displacements were larger than theoretical values due to slipping of the bolts at both ends and the deformation of the connection. Figure 14 depict the time histories for roof accelerations in the *X* and *Y* directions, respectively, for the structure with and without MC-BRBs under the tri-directional Chi-Chi earthquake. Comparative results from these figures illustrate that MC-BRBs can reduce the roof acceleration considerably under a tri-directional earthquake. Furthermore, comparisons of the roof displacement and the first floor column shear force responses in the *X* and *Y* directions between the structure, without and with MC-BRBs, subjected to the tri-directional Chi-Chi earthquake, are shown in Figs. 15 and 16, respectively. Comparative analysis shows that the added MC-BRBs reduced not only the roof displacement responses but also the first floor column shear forces. Therefore, it may be concluded that the structural responses can be effectively reduced during earthquakes by installing MC-BRBs.

Numerical simulations of the tested structure equipped with MC-BRBs under seismic loadings were performed using the computer program NSAT (Tsai, 1996) to predict the responses of the structure. In the numerical analyses (refer to Figs. 13 (a) and (b)), the beam elements with linearly elastic behavior and 12 degrees of freedom (DOFs) were adopted for simulating

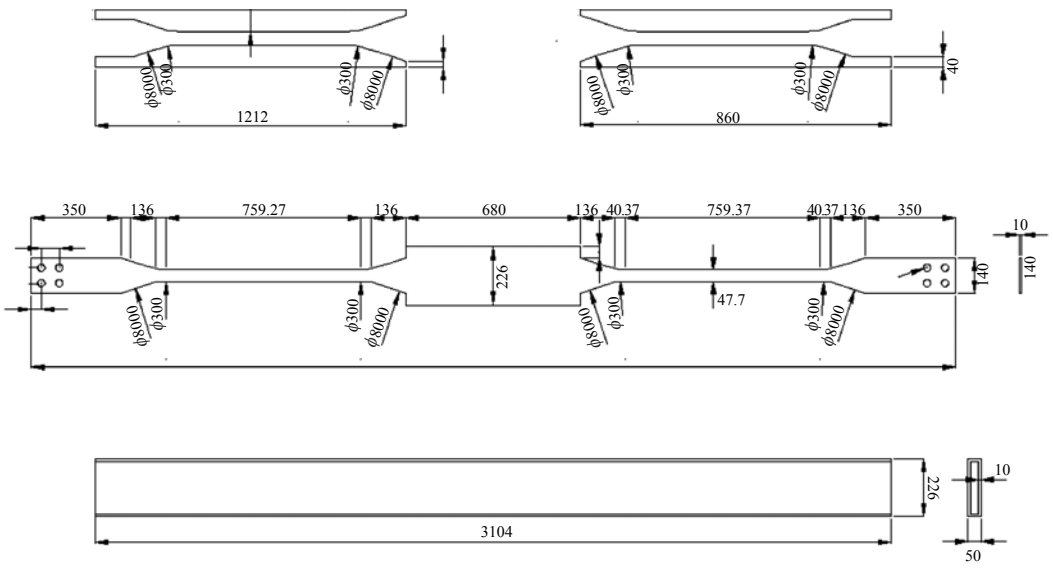

Fig. 11 Sketch of MC-BRB in *X*-direction in full scale steel structure (Length unit: mm)

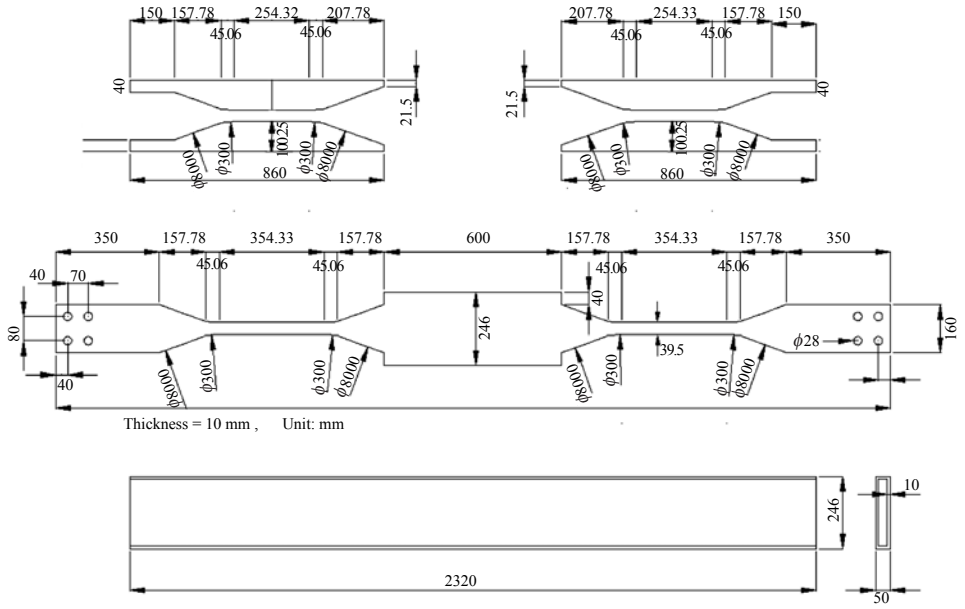

Fig. 12 Sketch of MC-BRB in *Y*-direction in full scale steel structure

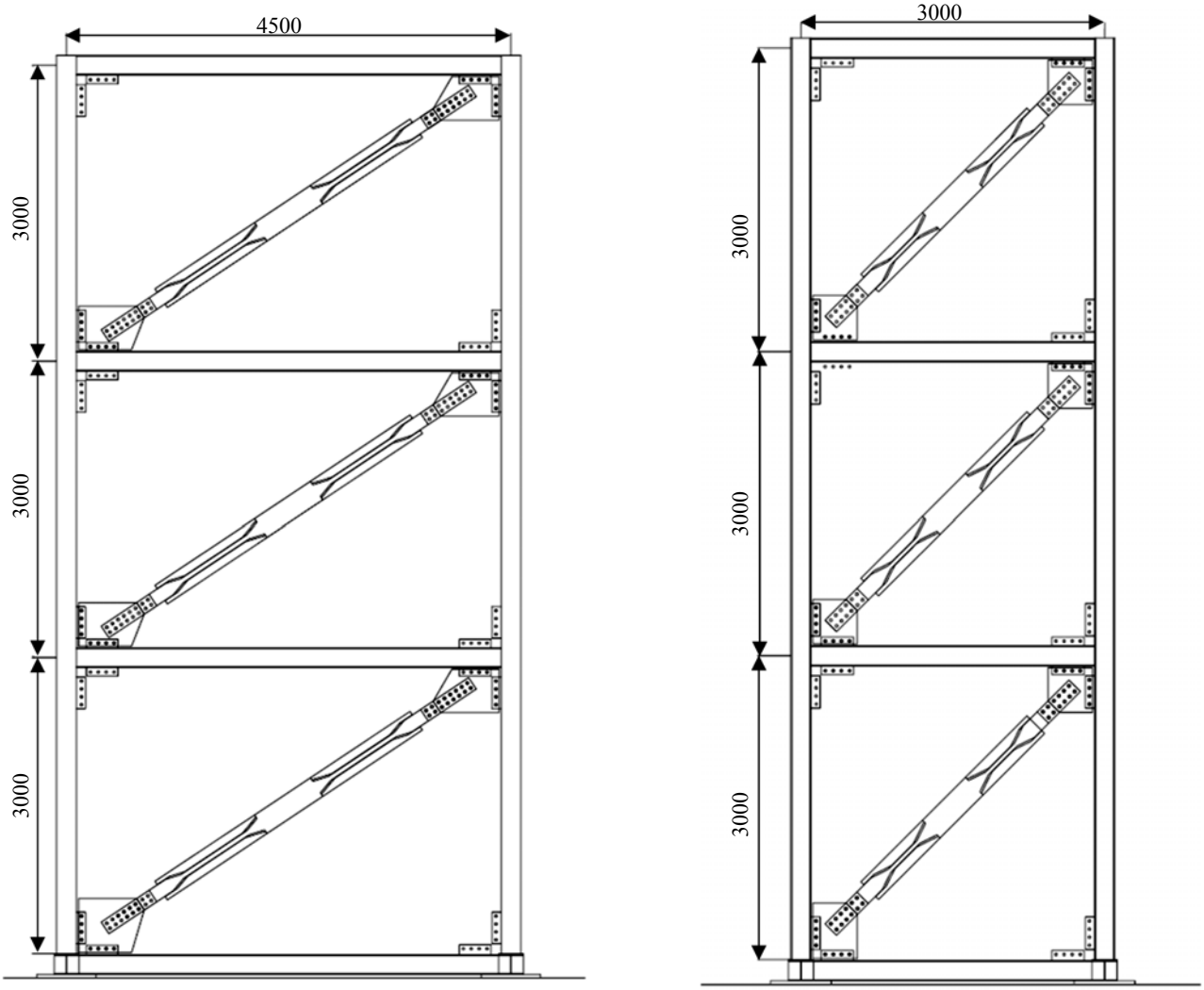

(a) In *X*-direction (b) In *Y*-direction

Fig. 13 Full scale steel structure equipped with MC-BRBs (Unit: mm)

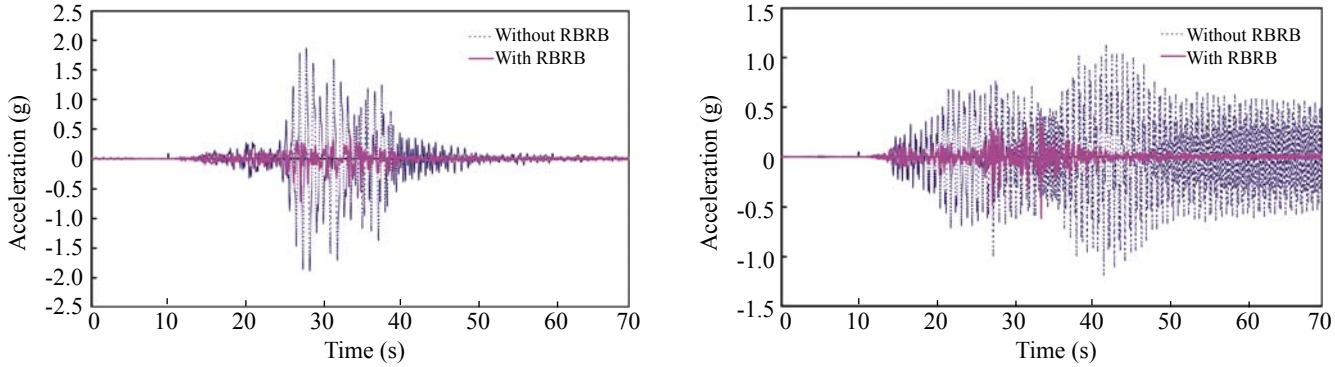

(a) *X*-direction (b) *Y*-direction

Fig. 14 Comparison of roof acceleration for structure with and without MC-BRB under Chi-Chi earthquake (TCU084 station, PGA = EW 0.5 g + NS 0.214 g + VER. 0.158 g)

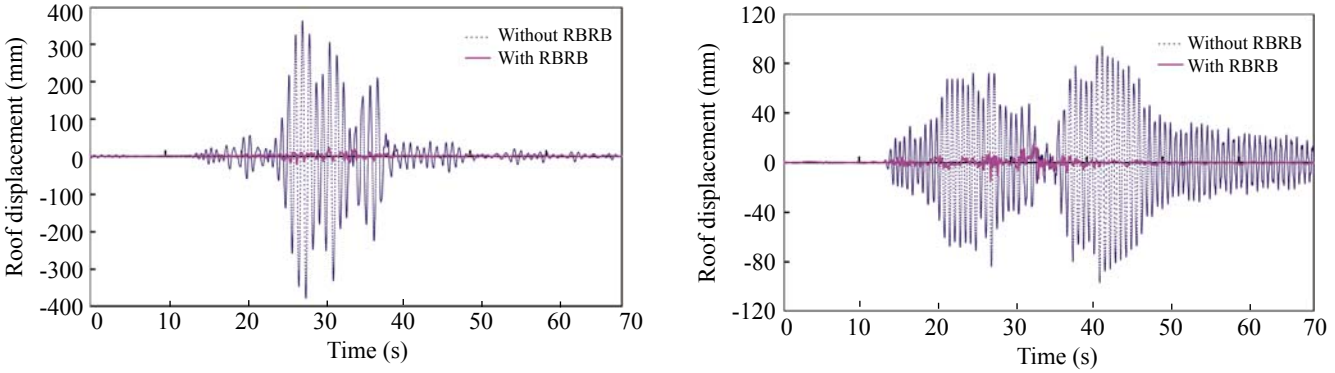

(a) *X*-direction (b) *Y*-direction

Fig.15 Comparison of roof displacement for structure with and without MC-BRB under Chi-Chi earthquake (TCU084 station, PGA = EW 0.5 g + NS 0.214 g + VER. 0.158 g)

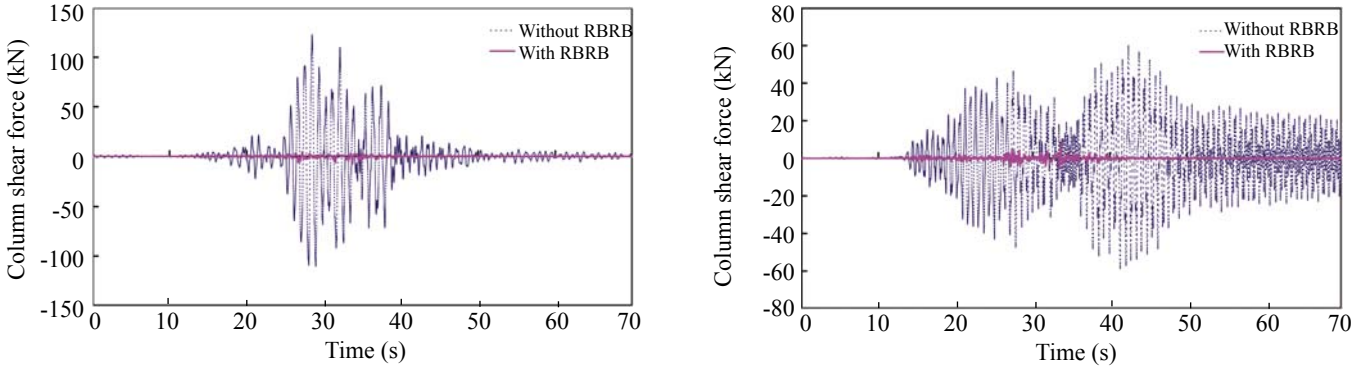

(a) *X*-direction (b) *Y*-direction

Fig. 16 Comparison of column shear force for structure with and without MC-BRB under Chi-Chi earthquake (TCU084 station, PGA = EW 0.5 g + NS 0.214 g + VER. 0.158 g)

beams and columns; the BRB elements with the plasticity model and 2DOFs previously derived in Section 3 were used for modeling MC-BRBs in the full-scale steel structure; and the boundary condition of a fixed base between the column and the foundation was assumed. Figures 17, respectively, present comparisons of the roof accelerations between the experimental and simulated results, for a structure subjected to two different ground motions. Comparative results showed that under earthquake conditions, the roof acceleration responses of the structure with MC-BRBs can be adequately predicted by the proposed mathematical model.

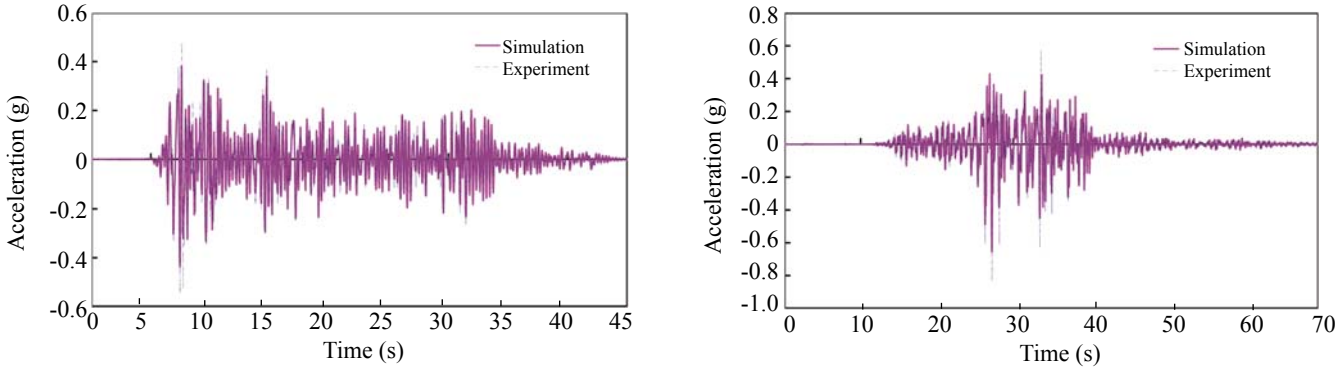

(a) Roof acceleration (0.3 g El Centro earthquake)

(b) Roof acceleration (0.5 g Chi-Chi earthquake)

Fig. 17 Comparison of roof acceleration in *X*-direction for experiment and simulation under El Centro and Chi-Chi (TCU084) earthquake

6 Conclusions

The traditional BRBs, with mortar filling in a steel tube to prevent the core plate from buckling, have been extensively employed in Japan and the U.S. However, manufacturing procedures are complex due to the many interfaces needed for different materials and the time-consuming process of fabricating and strengthening the mortar. Also, quality control is difficult and cannot be assured beforehand, without testing during the manufacturing process and after earthquakes.

With the objective of overcoming the disadvantages of traditional BRBs, the multi-curve buckling restrained brace (MC-BRB) is proposed in the present study. This new device, using steel materials, considerably simplifies the manufacturing process. The MC-BRB has been validated through component tests that showed that the proposed system exhibits stable mechanical behavior. Furthermore, the two-surface model can reliably predict the behavior of the MC-BRBs under both cyclic and seismic loading. In addition, the experimental results from a full-scale, three-story steel structure equipped with MC-BRBs under tri-directional earthquakes illustrate that they can effectively reduce most of the responses in a structure during earthquakes.

Acknowledgement

Financial support for this study has been provided by the Science Council in Taiwan (Project No. NSC 94-2211-E-035-015). Special thanks to the Council for providing the financial support to complete this project.

References

Black CJ, Makris N and Aiken ID (2002), "Component Testing, Stability Analysis and Characterization of Buckling-restrained Braces," *Journal of Structural Engineering*, ASCE, **130**(6): 880–894.

Black CJ, Makris N and Aiken ID (2004), "Component Testing, Seismic Evaluation and Characterization of Buckling-restrained Braces," *Report No. PEER-2002/08*, Pacific Earthquake Engineering Research Center, University of California, CA

Kimura K, Yoshizaki K and Takeda T (1976), "Tests on Braces Encased by Mortar In-filled Steel Tubes," *Summaries of Technical Papers of Annual Meeting, Architectural Institute of Japan,* pp.1041–1042 (in Japanese).

Ma N, Wu B, Zhao J, Li H, Ou J and Yang W (2008), "Full-scale Test of All-steel Buckling Restrained Braces," *14th World Conference on Earthquake Engineering*, Beijing, China, October 12–17, 2008; Paper No. 11-0208.

Merritt S, Uang CM and Benzoni G (2003), "Subassemblage Testing of Corebrace Buckling-Restrained Braces," Department of Structural Engineering, UC San Diego, Structural Systems Project, *Report No. TR-2003/01*.

Phillips A and Lee CW (1979), "Yield Surfaces and Loading Surfaces: Experiments and Recommendations," *International Journal of Solids and Structures*, **15**: 715–729.

SEAOC-AISC (2002), "Recommended Provisions for Buckling-restrained Braced Frames," *Draft*, SEAOC and AISC.

Tsai CS (1996), "Nonlinear Stress Analysis Techniques," Department of Civil Engineering, Feng Chia University, Taichung, Taiwan.

Tsai CS and Chen KC (2004), "Nonlinear Analyses of Structures with Added Passive Sevices," *Structural Engineering and Mechanics,* An International Journal, **18**(4): 517–539.

Tsai CS, Chen WS and Chen KC (2005), "Shaking Table Test of Structure with Reinforced Buckling Restrained Braces," Seismic Engineering*, The 2005 ASME PVP Conference*, Denver, Colorado, U.S.A., July 17-21, **8**: 307–312.

Tsai CS, Chen WS and Chen BJ (2006), "Component Tests and Simulation of Advanced Buckling Restrained Braces," Seismic Engineering, *The 2006 ASME PVP Conference*, Vancouver, BC, Canada, July 23-27, Paper No. PVP2006-ICPVT11-93491.

Tsai CS, Chen WS and Lin YC (2008), Full-scale Shaking Table Tests of a Steel Structure with Multi-Curve Buckling Restrained Braces," *14th World Conference on Earthquake Engineering*, Beijing, China, October 12-17, 2008; Paper No. 05-06-0007.

Tsai CS, Chiang TC, Chen BJ, Chen WS and Yu SH (2004), "Component Test and Mathematical Modeling of Advanced Unbonded Brace," Seismic Engineering, *The 2004 ASME PVP Conference*, San Diego, California, **486**(2): 231–236.

Tseng NT and Lee GC (1983), "Simple Plasticity Model of Two-surface Type," *Journal of Engineering Mechanics*, ASCE, **109**(3):795–810.

Wada A, Connor J, Kawai H, Iwata M and Watanabe A (1992), "Damage tolerant structures," *Proceeding 5th U.S.-Japan Workshop on the Improvement of Structural Design and Construction Practices*, San Diego, CA, Applied Technology Council, ATC-15-4: 27–39.

Wakabayashi M, Nakamura T, Kashibara A, Morizono T and Yokoyama H (1973), "Experimental Study of Elasto-plastic Properties of Precast Concrete Wall Panels with Built-in Insulating Braces," *Summaries of Technical Papers of Annual Meeting, Architectural Institute of Japan*, Structural Engineering Section **10**: 1041–1044 (in Japanese).